MALAYSIAN JOURNAL OF SCIENCE
MJS
ISSN 1394-3065

Regular Issue

Malaysian Journal of Science 43 (3): 59-67 (September 2024) https://mjs.um.edu.my

MATHEMATICAL MODEL OF NICKEL-GRAPHENE COMPOSITE INKS FOR JETTING PROPERTIES IN INKJET PRINTING

Neha Thakur[1a]*, Parasuraman Swaminathan[2b], Hari Murthy[3a]

Abstract: The droplet formation process in inkjet printing is studied numerically and verified through a simulation model. The droplet formation process decides the printing quality of the coating, and a mathematical model is developed to understand the complete process from droplet formation to detachment. The Navier-Stokes equation is used to mathematically derive the droplet radius ($r_{numerical}$). COMSOL multiphysics is used for simulation and the radius ($r_{simulation}$) is calculated from the droplet mass. The $r_{numerical}$ and $r_{simulation}$ are compared for inks containing nickel, graphene, and nickel-graphene composite ink it is observed that the composite ink radiuses have the lowest difference ($r_{simulation}$ - $r_{numerical}$ = 0.085 µm). A droplet is formed at 1.47 mm from the nozzle inlet, for nickel-graphene ink, and after 1.5mm for other pristine inks. The results are verified through Z number, velocity profile, and droplet mass. The droplet formation observed from the velocity profile is earliest at 120 µs. It is seen that a stable droplet is generated at 100µs for nickel-graphene ink and at 200 µs for individual inks.

Keywords: *Drop formation, inkjet printing, COMSOL multiphysics, composite ink, nickel-graphene ink.*

1. Introduction

Inkjet Printing (IJP) is one of the material printing techniques that has shown remarkable throughput in recent years. Printing technology is preferred over other conventional deposition techniques because of their lower deposition time, compactness, reduced number of patterning steps, and adaptation to different substrates. Farraj et al., (2014) discussed two types of IJP techniques that have been developed: continuous inkjet (CIJ) and drop-on-demand (DOD), wherein the former, continuous ink flow occurs, and droplets are formed irrespective of whether the character is available or not. CIJ can print features up to 20-50 µm with a preferred viscosity of up to 16 mPa.s. In DOD, the droplet is formed only when the character is present resulting in lower resource wastage. The viscosity range for DOD lies between 20-40 mPa.s. According to Hoath et al., (2016), each droplet maintains a ligament that prolongs from the main droplet body towards the nozzle. The main functioning of the IJP relies on droplet formation, which in turn depends on the ink's rheological properties (viscosity, surface tension, and density). The ink contains active agents, precursors, dispersing medium, and surfactants, which must be selected appropriately as suggested by Murthy et al. (2021). The droplet generation process is divided into four stages - droplet generation, flight mode, drop impingement, and drop hardening. A droplet is said to be generated when the fluid mass accumulated exceeds the surface tension force that holds the fluid onto the surface. A behavior change occurs because the liquid drop takes a shape that minimizes the free energy (ψ) of the system, contributed by the three interfaces (solid, liquid, and gas), given by Kulkarni et al., (2016):

$$\psi = \sigma_{LS} A_{LS} + \sigma_{SG} A_{SG} + \sigma_{LG} A_{LG} \quad (1)$$

σ_{LS}, σ_{LG}, and σ_{SG} are the surface energy for liquid-solid, liquid-gas, and solid-gas interface, respectively. A_{LG}, A_{LS}, and A_{SG} are the areas of liquid-gas, liquid-solid, and solid-gas interface, respectively.

For a homogenous surface, the surface tension should be balanced as:

$$\sigma_{SG} = \sigma_{LS} + \sigma_{LG} \cos\phi_{eq} \quad (2)$$

where, ϕ_{eq} represents the equilibrium contact angle, given as the angle between the liquid/gas interface as it meets the solid surface.

$$\cos\phi_{eq} = \frac{\sigma_{SG} - \sigma_{LS}}{\sigma_{LG}} \quad (3)$$

Drop impingement occurs when a droplet hits the substrate and the extent of surface wetting is determined by ϕ_{eq}. The droplet behavior varies from equilibrium or stable state to spread, recede, rebound, partial rebound, and oscillate depending upon the wetting conditions discussed by Davydzenka et al., (2016) as given in **Table** 1. The splashing of the droplet is determined by the Weber number (We) and Reynold's number (Re) used for determining the Z-number. Z-number is used to confirm the ink printability. The ideal values for the Z number are between 1-10, where below 1, the fluid will not flow because of insufficient energy, and for Z >10, the fluid will too viscously be creating satellite droplets. The ideal relation between Re and We for inkjet printing applications is defined by Derby (2015) as given in Figure 1.

Authors information:
[a]Dept. of Electronics and Communication Engineering, CHRIST (Deemed to be University), Bengaluru, Karnataka, INDIA.
[b]Dept. of Metallurgical and Materials Engineering, Indian Institute of Technology, Madras, Tamil Nadu, INDIA.
*Corresponding Author: neha.thakur@res.christuniversity.in

Received: July 21, 2023
Accepted: October 23, 2023
Published: September 30, 2024

DOI:https//doi.org/10.22452/mjs.vol43no3.8
Malaysian Journal of Science 43(3): 59-67 (September 2024)

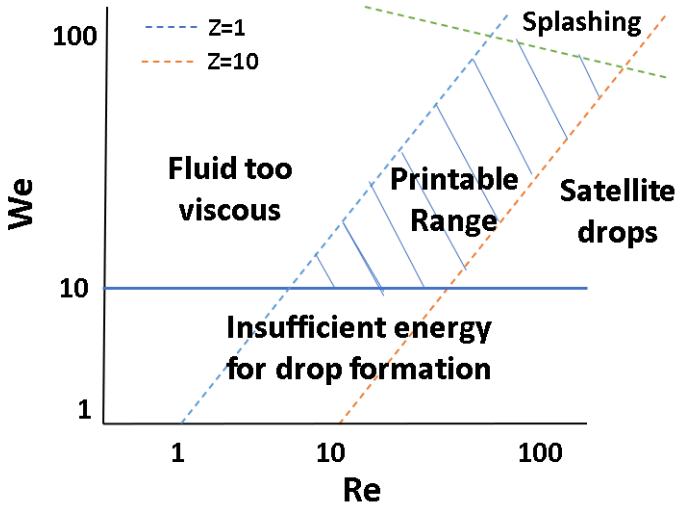

Figure 1. Relationship between Re and We which influences the ink printability.

Table 1. Wetting conditions for different contact angles

ϕ_{eq}	Expression	Wettability	Example
0	$\sigma_{LG}= \sigma_{SG}- \sigma_{LS}$	Complete wetting	
0 to 90º		Partial wetting	
90º	$\sigma_{SG} = \sigma_{LS}$	Equilibrium	
90º to 180º		Partial non-wetting	
180º	$\sigma_{LG}= \sigma_{LS} - \sigma_{SG}$	Non-wetting	

The proposed work involves a mathematical multiphase (liquid ink and air) fluid flow model. The model is developed to determine the droplet's behavior during formation and travel toward the substrate. To date, the droplet radius is not calculated mathematically as per the author's knowledge, and the proposed work will be helpful for users working on coating techniques like inkjet printing. The droplet radius is calculated and the input parameters are varied to predict the droplet radius prior to printing. As a case study, nickel-graphene ink has been used for simulation in the literature. Nickel-graphene composites exhibit strong sp^2 hybridization between the 2p orbital of graphene and the 3d orbital of nickel with a low lattice mismatch of ~1.2% and an inter-metal separation of 0.21 nm. The strong chemical interaction between graphene and nickel makes it an excellent electrical conductor for electronic applications summarized by Thakur et al., (2021). Takuya et al., (2023) derived a model to determine the breakup length of the droplet stream from the ligament.

DOI:https//doi.org/10.22452/mjs.vol43no3.8
Malaysian Journal of Science 43(3): 59-67 (September 2024)

2. Materials and Methods

The fluid interface and convection with air are represented as part of a laminar two-phase flow, by considering the level set method, considering the inks as Newtonian fluid. Mathematical and simulation models are used to obtain droplet radius for multiphase flow (MPF). Before realizing the MPF model, the single-phase flow (SPF) model is derived.

Single Phase Flow (SPF)

Figure 2 shows the channel area where the fluid flow occurs is considered a cylindrical coordinate (r, θ, z), where 'r' is the nozzle radius, 'θ' is the angle between the reference direction (z) on the chosen plane and the line from the origin to the projection on the plane, and 'z' is the distance from the inlet to the point of reference. Assuming that the direction of fluid flow is in z-direction towards the substrate, implies v_r =0, v_θ =0, and that there is no effect of gravity. The Navier Stokes (NS) equation is written by Rev et al., (2018):

$$\rho\left(\frac{\partial \vec{v}}{\partial t} + (\vec{v}.\vec{\nabla})\vec{v}\right) = -\vec{\nabla}P + \mu\nabla^2\vec{v} \tag{4}$$

where, 'μ' is viscosity (mPa.sec), 'ρ' is density (kg/m^3), 'P' is pressure (Pa), and 'v' is velocity (m/sec).

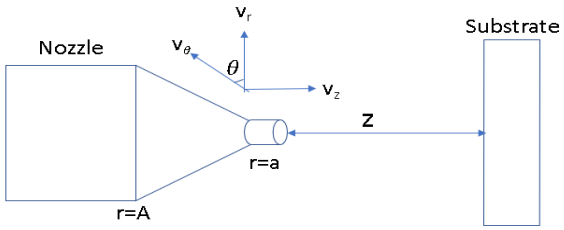

Figure 2. The cylindrical coordinate system for the proposed nozzle schematics

Solving the above NS equation for the 'r' coordinate and 'θ' based on the condition that v_r =0, v_θ =0, we get:

$$-\frac{\partial P}{\partial r} = 0 \tag{5}$$

and

However, solving for the 'z' coordinate, we get:

$$-\frac{1}{r}\frac{\partial P}{\partial \theta} = 0 \tag{6}$$

$$\frac{\partial P}{\partial z} = \mu\left[\frac{1}{r}\frac{\partial}{\partial r}\left(r\frac{\partial v_z}{\partial r}\right)\right] = constant \tag{7}$$

If P_1 is the inlet pressure, P_2 is the outlet pressure, with L being the surface length, then for the ink to flow across the 'z' direction P_1 should be greater than P_2, and the pressure gradient is given as:

$$\frac{\Delta P}{L} = -\mu\left[\frac{1}{r}\frac{d}{dr}\left(r\frac{dv_z}{dr}\right)\right] \tag{8}$$

The velocity in the z direction, v_z is obtained:

$$v_z = -\frac{1}{2\mu}\frac{\Delta P}{L}\frac{r^2}{2} + C_1\ln(r) + C_2 \tag{9}$$

The boundary conditions for single-phase flow are given as:

- No slip condition at the wall, i.e., $\frac{dv_z}{dr} = 0$ (r=a)
- No fluid velocity at the outer radius of the nozzle, i.e., v_z= 0 (at r=A)

Applying the boundary conditions to obtain the constants C_1 and C_2, we get

$$C_1 = \frac{1}{2\mu}\frac{\Delta P}{L}a^2 \tag{10}$$

$$C_2 = \frac{1}{2\mu}\frac{\Delta P}{L}\left(\frac{A^2}{2} - a^2\ln(A)\right) \tag{11}$$

Thus, the generalized velocity for SPF is obtained as:

DOI:https//doi.org/10.22452/mjs.vol43no3.8
Malaysian Journal of Science 43(3): 59-67 (September 2024)

$$v_z(r) = -\frac{1}{2\mu}\frac{\Delta P}{L}\left[\frac{r^2}{2} - a^2\ln(r) - \frac{A^2}{2} + a^2\ln(A)\right] \quad (12)$$

The volume flow rate is calculated as:

$$Q = \frac{\pi}{8\mu}\frac{\Delta P}{L}(A^2 - a^2)(A^2 - 3a^2) \quad (13)$$

Multiphase Flow (MPF)

Two phases are considered for deriving the numerical model having velocities v_{z1} and v_{z2}, pressure P_1 and P_2, viscosities μ_1, and μ_2 for the phase 1 and phase 2 respectively, 'r' is the variable radius of the flow across the length of the nozzle, 'R_d' is the radius of the fluid flow. The velocities for phase 1 and phase 2 are given as:

$$v_{z1} = -\frac{1}{2\mu_1}\frac{\partial P_1}{\partial z}\frac{r^2}{2} + C_{11}\ln(r) + C_{21} \quad (14)$$

$$v_{z2} = -\frac{1}{2\mu_2}\frac{\partial P_2}{\partial z}\frac{r^2}{2} + C_{12}\ln(r) + C_{22} \quad (15)$$

The boundary conditions for multiphase flow are given as:

- No slip condition at the wall, i.e., v_{z1}=0 (r=a)
- At the starting point, there is no change in the velocity, i.e., $\frac{dv_{z2}}{dr} = 0$ (at r=0)
- Same travel velocity for the two fluids, i.e., v_{z1} (R_d)= v_{z2} (R_d)
- Constant shear stress for both fluids, i.e., $\zeta_1(R_d) = \zeta_2(R_d)$

Applying the boundary conditions to obtain the following constants:

$$C_{21} = \frac{1}{2\mu_1}\frac{\partial P_1}{\partial z}\frac{a^2}{2} - C_{11}\ln(a) \quad (16)$$

$$C_{12} = 0 \quad (17)$$

$$C_{11} = \frac{V_{tp} + \frac{1}{4\mu_1}\frac{\partial P_1}{\partial z}\left({R_d}^2 - a^2\right)}{ln\left(\frac{R_d}{a}\right)} \quad (18)$$

$$C_{22} = \frac{1}{2\mu_2}\frac{\partial P_2}{\partial z}\frac{{R_d}^2}{2} + V_{tp} \quad (19)$$

$$C_{21} = \frac{1}{2\mu_1}\frac{\partial P_1}{\partial z}\frac{a^2}{2} - \frac{4V_{tp} + \frac{\partial P_1}{\partial z}\left({R_d}^2 - a^2\right)}{4\mu_1\, ln\left(\frac{R_d}{a}\right)}ln(a) \quad (20)$$

After substituting the values of all constants, velocities and flow rates of the two phases are given by Li et al., (2021):

$$v_{z1} = -\frac{1}{2\mu_1}\frac{\partial P_1}{\partial z}\frac{r^2}{2} + \frac{4V_{tp} + \frac{\partial P_1}{\partial z}\left({R_d}^2 - a^2\right)}{4\mu_1\, ln\left(\frac{R_d}{a}\right)}ln\left(\frac{r}{a}\right) + \frac{1}{2\mu_1}\frac{\partial P_1}{\partial z}\frac{a^2}{2} \quad (21)$$

$$v_{z2} = -\frac{1}{2\mu_2}\frac{\partial P_2}{\partial z}\frac{r^2}{2} + \frac{1}{2\mu_2}\frac{\partial P_2}{\partial z}\frac{{R_d}^2}{2} + V_{tp} \quad (22)$$

$$Q_1 = \frac{\pi}{\mu_1}\left\{\left[\frac{\partial P_1}{\partial z}\left(\frac{{R_d}^2 - a^2}{2}\right)\left[\frac{{R_d}^2 - a^2}{4} - E_1\right] - \frac{E_1}{2}\right]\right\} \quad (23)$$

$$Q_2 = \pi\left\{\frac{1}{\mu_2}\frac{\partial P_2}{\partial z}\frac{{R_d}^4}{8} + {R_d}^2 V_{tp}\right\} \quad (24)$$

The droplet formation process is derived with respect to fluid velocity (v_z) and volume flow rate (Q). The numerical droplet diameter ($d_{numerical}$) and radius ($r_{numerical}$) as the function of nozzle diameter (d_N) and nozzle radius (r_N) respectively and also the function of volume flow rate, is given as:

DOI:https//doi.org/10.22452/mjs.vol43no3.8
Malaysian Journal of Science 43(3): 59-67 (September 2024)

$$d_{numerical} = d_N \sqrt[3]{\left(1 - \frac{6Q_2}{\pi Q_1}\right)} \quad (25)$$

$$r_{numerical} = r_N \sqrt[3]{\left(1 - \frac{6Q_2}{\pi Q_1}\right)} \quad (26)$$

Simulation Model

The drop-on-demand process uses COMSOL multiphysics software to understand the different stages involved in the droplet formation process. Due to the nozzle geometry, an axis-symmetric 2D model is used to simplify the calculations. Initially, the space between the nozzle and the substrate is filled with air. The ink is ejected through the nozzle and forced to flow out of the nozzle forming a droplet that eventually changes shape and cuts off from the nozzle. The droplet is constantly changing shape and travels towards the substrate. The properties of the fluid are expected to be different in the nanochannel in comparison to the bulk which is given by Rudyak et al., (2011). The adaptive mesh refinement functionality of COMSOL multiphysics is used to refine the mesh around the ink and air interface. A similar model is developed by Tofan et al., (2022) for modelling 3D droplet movement using a DoD inkjet printhead model. The functionality divides the simulation into several time intervals and locally refines the mesh in the region where the phase interface is present in each interval to increase calculation accuracy.

The following assumptions are made to simplify the simulation process

1. The fluid and surrounding air are incompressible.
2. Heat transfer will be neglected, and the ink will be assumed to have constant properties throughout the problem. No liquid evaporation takes place.
3. Laminar flow
4. The liquid properties are constant with time.

The droplet size and velocity are controlled during the ejection by applying a rectangular function as shown in **Figure 3** to the inlet velocity forcing a pressure increase inside the modelled nozzle. It helps to set the pulse length and maximum inlet fluid velocity magnitude, which affects the resulting velocity of the ejected droplet, though magnitude has a larger influence on the droplet velocity. The nozzle geometry is created using the dimensions given in **Table 2** and is shown in **Figure 4**.

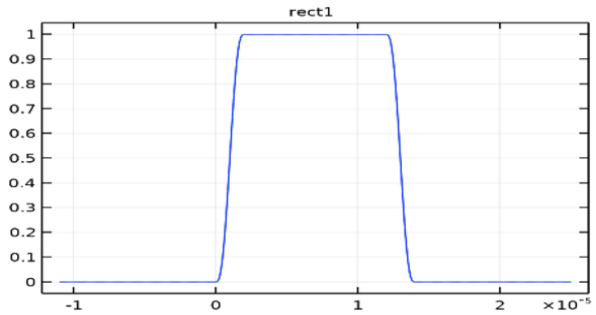

Figure 3. Rectangular function of the increasing pressure in the nozzle

Table 2. Dimensions of the nozzle geometry used for simulation

Name	Value (μm)
Inlet Radius	100
Nozzle Length	375
Nozzle Radius	25
Throat Length	25
Distance to target	1000
Air Channel Width	100

DOI:https//doi.org/10.22452/mjs.vol43no3.8
Malaysian Journal of Science 43(3): 59-67 (September 2024)

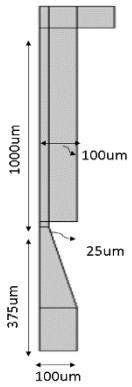

Figure 4. Nozzle geometry used for simulation model

The boundary condition selected for simulation is the same as for the fully developed flow. According to the COMSOL Module User's guide by Burlington et al., (2018), the level set method is selected, and the value for the level set function (ϕ) is '0' for the air and '1' for ink. In the transition layer close to the interface, ϕ goes from 0 to 1 smoothly, with the interface moving together with the fluid velocity. For the simulation, the physics-controlled mesh has been used with a minimum element size of 3.18 μm, and a curvature factor of 0.3. The wetted wall conditions used were the wall condition used was Navier slip, slip length 10 μm, and the contact angle as pi/2. The range used for computation was (0, 10 x 10^{-6}, 500 x 10^{-6}) using a PARDISO solver. From the simulation report, droplet mass is obtained, which is further used to calculate the droplet radius. The material properties used for simulation are given in **Table 3**.

Table 3. Material properties used for simulation

Material	Density (kg/m^3)	Surface Tension (mN/m)	Viscosity (mPa.s)
Air	1		
Graphene	1300	10	33.45
Nickel	7810	72	44

3. Results and Discussion

The droplet formed for all inks along with its position and formation time is given in **Table 4**. It can be seen from the simulation model; that the droplet is formed earliest at 1.47 mm from the nozzle inlet in the nickel-graphene ink.

Table 4. Droplet formation in the simulation model

Ink	Nickel	Graphene	Nickel-graphene
Result	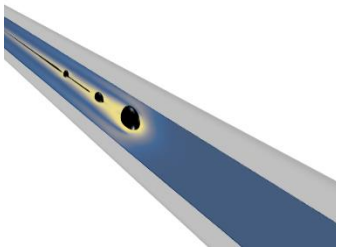	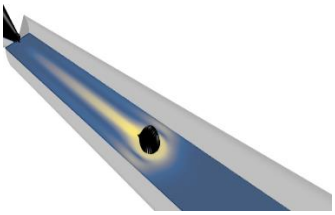	
Droplet position	@1.5456mm	@2.667mm	@ 1.47mm
Time	20μs	20μs	20μs

Viscosities and surface tension for nickel ink and graphene ink are shown in **Table 5**. For each value, the numerical and simulation droplet radius is calculated and compared. The case with the least difference (nickel viscosity 44 mPa.sec, graphene viscosity 33.4 mPa.sec) in the radius values is chosen for further analysis.

DOI:https//doi.org/10.22452/mjs.vol43no3.8
Malaysian Journal of Science 43(3): 59-67 (September 2024)

Table 5. Numerical and simulation radius calculated for the existing rheological properties from the literature

Ink used	Viscosity (mPa.s)	Surface Tension (mN/m)	Oh	Mass (μg)	Numerical radius(μm)	Simulation Radius (μm)	Ref
Liquid nickel	44	72	0.166	0.21	39.86	41.67	Cherne et al. (2002)
Ni ink	25	15	0.207	0.2	39.21	41.66	Altay et al., (2018)
NiO nano fluid	22.4	45.9	0.106	0.2	39.22	41.66	Ramachandran et al., (2020)
Graphene ink	43.5	15	0.402	0.2	71.30	41.67	Chen et al., (2020)
Graphene ink	15	72	0.14	0.22	73.60	41.67	Secor et al., (2015)
Graphene ink	33.4	10	0.83	0.2	41.67	41.97	Gao et al., (2014)

Nickel-graphene (Ni-G) composite ink is considered and the radius is calculated to be around ~41.66 µm which is close to the simulated radius of 41.67 µm. The density, viscosity, and surface tension of the nickel-graphene ink were taken as 4555 kg/m^3, 38.87 mPa.s, and 72 mN/m respectively. The droplet mass was found to be 14x10^{-11} kg. It is observed that Ni-G ink composite gives better results in comparison to the individual inks. It is discernible that all three inks are coming in the printability range of 1 to 10.

There is continuous change in the fluid velocity and to understand the exact fluid flow mechanism with respect to velocity five points (A, B, C, D, and E) are considered at different time intervals from 20 to 180μs. The mechanism at each point of time is described in **Table 6**. It is apparent that Ni-G composite ink droplets are detached earliest at 1.124 mm as shown in **Figure 5**.

Table 6. Velocities at different stages of droplet formation for nickel, graphene, and nickel-graphene composite

	Significance	Time (μs)	Ni (m/s)	G (m/s)	Ni-G (m/s)
A	The droplet is ejected from the nozzle with maximum pressure	20	10	9.12	9.94
B	The droplet is followed by a ligament with maximum length, mass, and volume	80	9.79	8.72	9.03
C	Almost spherical droplet is formed	100	10.8	9.05	9.19
D	Droplet is detached	120	9.71	10.4	9.37
E	The droplet starts moving toward the substrate	180	9.49	9.5	9.05

The droplet mass is determined up to 500 μs, and the values are graphically represented in **Figure 6**. The droplet mass results are obtained from the droplet mass curve generated by COMSOL multiphysics. For Ni ink and graphene ink, the stable (or constant) droplet mass is achieved at 200 μs whereas for Ni-G composite ink the stable droplet mass is achieved at 100 μs. The emphasis is given on droplet mass because the droplet mass indicates the droplet volume and the radius can be calculated from the volume.

For Ni ink and graphene ink, the stable droplet mass is achieved at 200 μs whereas for Ni-G composite ink the stable droplet mass is achieved at 100 μs. The droplet mass remains fixed once the droplet is ejected from the nozzle.

DOI:https//doi.org/10.22452/mjs.vol43no3.8
Malaysian Journal of Science 43(3): 59-67 (September 2024)

Future work would be focused on understanding the impact of more parameters and deepening into the droplet behavior, along with the validation of the results through physical experimentation. The proposed numerical work as an implementation study with COMSOL is useful for scientists working on the modelling of inkjet printing. By using COMSOL, the numerical modelling of the motion of inkjet droplets has been achieved, and the length of the dropped thread, the moment when the drop is pulled out of the thread when the droplet forms a spherical shape, droplet mass, droplet volume, droplet conditions on impact, and the final state of the droplet can be studied. In addition, it is now possible to configure different nozzle parameters, and different ejection pressures, test different inks as well, and consider different ink precursors given by Tofan et al., (2021).

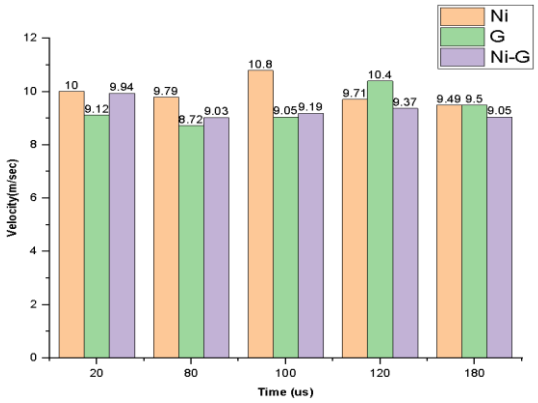

Figure 5. Velocity plot for nickel, graphene, and nickel-graphene composite. The graph indicates the velocity of droplets at different stages from ejection to detachment.
The nickel ink droplet is detached at 1.165mm, graphene at 1.248mm, and nickel-graphene ink composite at 1.124mm

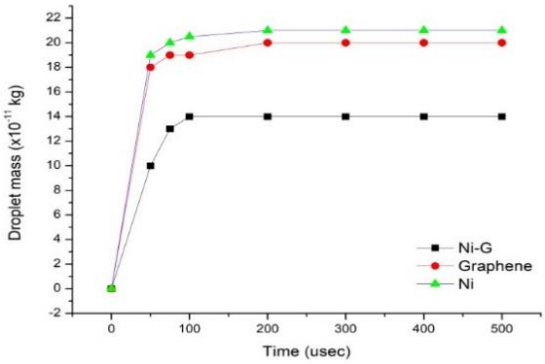

Figure 6. Droplet mass plot for nickel, graphene, and nickel-graphene composite

4. Conclusion

The droplet formation and detachment process are studied by modelling the inkjet nozzle numerically and through simulation. From both the models the droplet radius is derived and calculated. For verification purposes, three inks (Ni, G, and Ni-G) are chosen, and it is conspicuous that for Ni-G composite ink the difference in the droplet radius is 0.085 μm which is the least among all the three inks. Various analyses based on the Z parameter, velocity profile, and droplet mass are calculated for all the inks, and the most optimized results are obtained for the Ni-G ink composite. The stable droplet mass is achieved at 100μs for Ni-G ink whereas for others is obtained at 200μs and the droplet is formed earliest in Ni-G ink. Composite inks are expected to have better properties than their individual components and hence can play a crucial role in the future for various electronics and biosensing applications. In the future, the experimental work will be performed in three phases. The first phase includes ink formulation and characterization, keeping in mind the rheological properties of the present research. In the second phase, the formulated ink will be used to generate droplets and the droplets formed will be compared with the droplets in the simulation model. In the third phase, the droplet radius is calculated and will be compared with the numerical and simulation model.

5. Acknowledgements

I would like to express my deep and sincere gratitude to the Management at CHRIST (Deemed to be University), Bengaluru, and Dr. Inbanila K, Head, Department of Electronics and Communication Engineering for providing the necessary resources to complete the research.

6. References

Altay BN, Jourdan JS, Turkani VS, et al. (2018) Fundamental Mechanism of Ink Film Roughness The Impact of Substrate and Process on the Electrical Performance of Screen-Printed Nickel Electrodes. *ACS Appl. Energy Mater.* 1: 7164-7173

Burlington M. (2018) *CFD Module User's Guide; COMSOL*.

Chen H, Zhang Y, Ma Y, et al. (2020) Sand-Milling Exfoliation of Structure Controllable Graphene for Formulation of Highly Conductive and Multifunctional Graphene Inks. 12: 56319-56329

Cherne FJ, Baskes MI, Deymier PA. (2002) Properties of liquid nickel: A critical comparison of EAM and MEAM calculations. *Phys Rev B - Condens Matter Mater Phys*. 65.

Derby B. (2015) 3D Printing — Review Additive Manufacture of Ceramics Components by Inkjet Printing. *Engineering*. 1:113-123.

DOI:https//doi.org/10.22452/mjs.vol43no3.8
Malaysian Journal of Science 43(3): 59-67 (September 2024)

Farraj Y, Grouchko M, Magdassi S, Koch F., Wittkotter M., Muller M., Reinhold I., Zapka W. (2014). Ink-jet printed copper complex MOD ink for plastic electronics, *International Conference on Digital Printing Technologies*. 51: 1587-1590

Gao Y, Shi W, Wang W, Leng Y, Zhao Y. (2014) Inkjet printing patterns of highly conductive pristine graphene on flexible substrates. *Ind Eng Chem Res*. 53: 16777-16784.

Hoath S. D. (2016) Fundamentals of Inkjet Printing: The Science of Inkjet and Droplets. (Hoboken, ed.). *John Wiley & Sons.*

Kulkarni VS., Shaw C. (2016). Surfactants, Lipids, and Surface Chemistry. *Essent Chem Formul Semisolid Liq Dosages*

Li D (2001) *Interface Science and Technology*.

Murthy H., Thakur N., and NS. (2022). Nickel-Based Inks for Flexible Electronics - A Review on Recent Trends. *Journal of Adv Manuf Syst*. 21: 591-624.

Ramachandran H, Jahanara MM, Nair NM, Swaminathan P. (2020) Metal oxide heterojunctions using a printable nickel oxide ink. *RSC Adv*. 10: 3951-3959

Rev. BS. (2018) On the development of the Navier–Stokes equation byNavier. *Hist Phys Relat Sci*. 40: 1-12.

Rudyak V. Ya., Belkin (2011) A. A. Egorov V. V. IDA. Simulation of flows in nanochannels by the molecular dynamics method. *Nanosyst Physics, Chem Math*. 2:100-112.

Secor EB, Ahn BY, Gao TZ, Lewis JA, Hersam MC. (2015) Rapid and Versatile Photonic Annealing of Graphene Inks for Flexible Printed Electronics. *Adv Mater*. 27

Takuya O., Tsubouchi S., and Suwa Y. (2023). Analysis of the Ink-stream Break-Up Phenomenon in Continuous Inkjet Printing. *ACS Omega.* 8: 34442-34447.

Thakur N, Murthy H. (2021) Nickel-Based Inks for Inkjet Printing : A Review on Latest Trends. 11: 20-35.

Tofan T., Borodinas S., Kacianauskas R., and Jasevicius R. (2022). Modeling 3D Droplet Movement Using a Drop-on-Demand Inkjet Printhead Model. *Processes MDPI*: 10, 147.

Tofan Tim, Kruggel Emdem Harald, Turla Vytautas JR. (2021) Numerical Modeling of the Motion and Interaction of a Droplet of an Inkjet Printing Process with a Flat Surface. *Appl Sci*. 11: 527.

DOI:https//doi.org/10.22452/mjs.vol43no3.8
Malaysian Journal of Science 43(3): 59-67 (September 2024)